Statistical study of the subauroral polarization stream: Its dependence on the cross–polar cap potential and subauroral conductance

Hui Wang,[1,2] Aaron J. Ridley,[3] Hermann Lühr,[4] Michael W. Liemohn,[3] and Shu Y. Ma[1]

Received 23 June 2008; revised 4 August 2008; accepted 17 September 2008; published 30 December 2008.

[1] Two years of DMSP ion drift meter measurements have been used for a focused study of the subauroral polarization streams (SAPS). The main emphasis is on the effects of the cross–polar cap potential (CPCP) and the subauroral flux tube–integrated conductivity (that is, whether or not the northern and/or southern ionospheric footprint of the flux tube is sunlit or not) on the SAPS spatial distribution. For higher flux tube–integrated conductivity the SAPS tend to occur more poleward than for lower conductivity. The magnetic latitude (MLAT) difference can reach several degrees at most. The dependence of SAPS location on geomagnetic activity is also studied, and it is found that the SAPS magnetic latitude exhibits an exponential relation with *Dst*. When $Dst \leq -200$ nT the SAPS tend to occur at 48° MLAT. The CPCP averaged over 15 min prior to the SAPS correlates best with the SAPS peak velocities. The high-latitude CPCP has a stronger effect on the SAPS velocities for low integrated conductivity than for high conductivity. Finally, the observations show that there is a good anticorrelation between the subauroral integrated conductivity and the SAPS velocity, which confirms previous model results.

Citation: Wang, H., A. J. Ridley, H. Lühr, M. W. Liemohn, and S. Y. Ma (2008), Statistical study of the subauroral polarization stream: Its dependence on the cross–polar cap potential and subauroral conductance, *J. Geophys. Res.*, *113*, A12311, doi:10.1029/2008JA013529.

1. Introduction

[2] Subauroral polarization streams (SAPS) are one of the interesting and important features of the magnetosphere-ionosphere-thermosphere coupling. They represent rapid westward (sunward) plasma flows located equatorward of the auroral oval and predominantly in the dusk and premidnight sectors (1600–2400 magnetic local time (MLT)). They can change the ionospheric composition [*Anderson et al.*, 1991], lead to storm-enhanced density and plasmaspheric plumes [*Foster et al.*, 2002], produce very large field-aligned vertical flows [*Anderson et al.*, 1991], and form the *F* region density troughs [*Spiro et al.*, 1978].

[3] Previous studies have reported the characteristics and morphologies of SAPS by using measurements from satellites and radars [e.g., *Galperin et al.*, 1974; *Spiro et al.*, 1979; *Anderson et al.*, 1991; *Yeh et al.*, 1991; *Fejer and Scherliess*, 1998; *Scherliess and Fejer*, 1998; *Foster and Vo*, 2002; *Figueiredo et al.*, 2004; *Jensen and Fejer*, 2007] and from magnetospheric simulations [e.g., *Garner et al.*, 2004; *Liemohn et al.*, 2005; *Zheng et al.*, 2008]. When $Kp \geq 4$ the SAPS in the premidnight sector form at 60° magnetic latitude (MLAT), span 3°–5° in latitude, and have an average peak amplitude of >900 m/s [*Foster and Vo*, 2002]. The occurrences of SAPS are associated with substorms and storms [e.g., *Spiro et al.*, 1979; *Anderson et al.*, 1993; *Karlsson et al.*, 1998; *Foster and Vo*, 2002; *Burke et al.*, 2000]. The most probable local time of SAPS is found during 2100 and 2300 MLT, being most prominent around 2200 MLT [*Karlsson et al.*, 1998]. During equinox the SAPS events occur most often at European longitudes (~30°E) [*Jensen and Fejer*, 2007]. The magnetic latitudes of SAPS are reported to be linearly related to the magnitudes of *Dst*, as resulting from studies of four severe magnetic storms with -422 nT $\leq Dst_{min} \leq -271$ nT [*Huang and Foster*, 2007]. The location of SAPS is conjugate to the peak ring current energy density and the R2 field-aligned currents (FACs) [e.g., *Yeh et al.*, 1991; *Foster and Vo*, 2002] and coincides with the equatorward edge of the ion plasma sheet [e.g., *Southwood and Wolf*, 1978; *Anderson et al.*, 1993; *Huang and Foster*, 2007].

[4] The SAPS location is the consequence of the interaction of the regional shielding electric field and the large-scale convection electric field [e.g., *Ebihara and Fok*, 2004]. Since the flux tube–integrated ionospheric conductivity can influence the degree of the shielding electric field, which is the prime mechanism to deform the convection electric field, it is expected that this integrated ionospheric

[1]School of Electronic Information, Wuhan University, Wuhan, China.
[2]Formerly at Department of Atmospheric, Oceanic and Space Sciences, University of Michigan, Ann Arbor, Michigan, USA.
[3]Department of Atmospheric, Oceanic and Space Sciences, University of Michigan, Ann Arbor, Michigan, USA.
[4]GeoForschungsZentrum, Potsdam, Germany.

0148-0227/08/2008JA013529

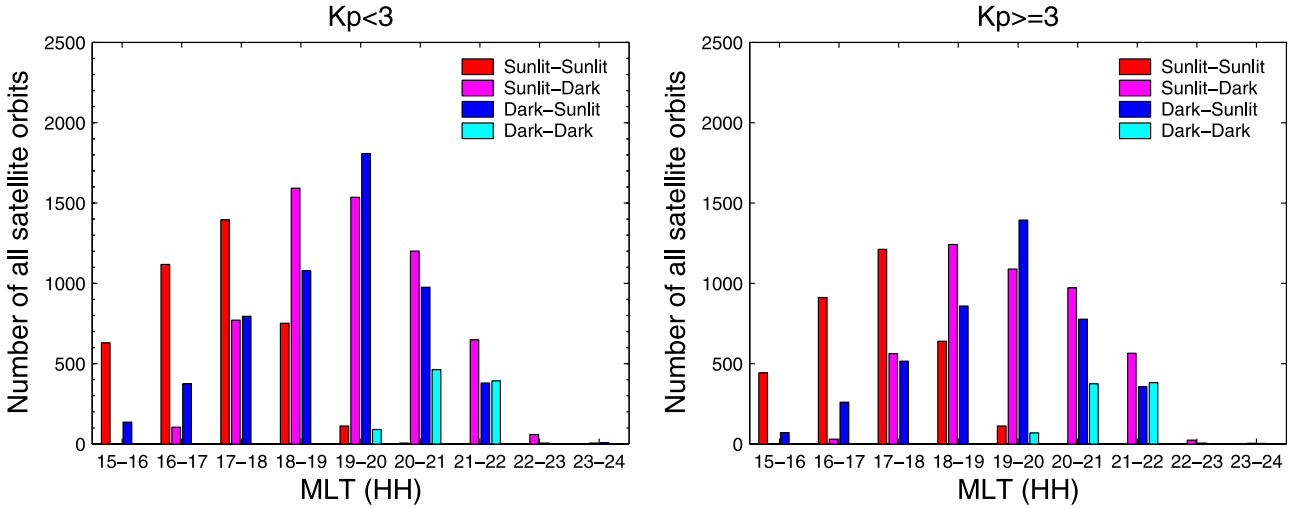

Figure 1. Number of satellite orbits in the premidnight sector as a function of MLT for two different geomagnetic activity levels, separately for four illumination conditions: (1) Northern Hemisphere (NH) sunlit, Southern Hemisphere (SH) sunlit (red); (2) NH sunlit, SH dark (magenta); (3) NH dark, SH sunlit (blue); and (4) NH dark, SH dark (cyan).

conductivity will affect the location of SAPS. Previous results have investigated extensively the solar illumination induced–ionospheric conductivity on the FACs and substorm onset locations [e.g., *Liou et al.*, 2001; *Christiansen et al.*, 2002; *Wang et al.*, 2005a, 2005b]. In contrast, the change in latitude of SAPS in response to solar illumination has so far not been investigated by utilizing observational techniques.

[5] The subauroral conductivity has been recognized to be approximately inversely proportional to the SAPS velocity [e.g., *Anderson et al.*, 1991]. Recent model studies have shown some interesting relationships between the conductivity and SAPS velocity. For example, *Zheng et al.* [2008] have presented a quantitative analysis of the relationship between the conductivity and SAPS by using the Comprehensive Ring Current Model (CRCM). They found that the magnitudes of the SAPS velocity decrease nonlinearly with the increasing conductivity. These model results need to be validated by observations. This study will try to investigate the possible effect of the flux tube–integrated conductivity on the SAPS velocities by using observations.

[6] The R2 FACs (shielding current) are another important factor that specifies the SAPS pattern [*Anderson et al.*, 2001]. The R2 FACs, when closing through the less conductive subauroral region to the high-latitude R1 FACs generate the SAPS. The R2 FACs are interrelated with the high latitudes through the electric field induced by the solar wind [*Anderson et al.*, 1993; *Liemohn et al.*, 2001; *Ridley and Liemohn*, 2002]. Enhanced convection electric fields can accelerate particles more deeply into the inner magnetosphere and generate much stronger R2 FACs. Therefore, the magnitude of the SAPS can be affected by the high-latitude electric field. However, statistical studies are so far lacking concerning the quantitative relationship between the high-latitude electric fields and the SAPS velocities. In this paper, we investigate SAPS dependence on the high-latitude electric field, represented by the cross–polar cap potential (CPCP), the subauroral conductivity, and geomagnetic activity, by using 2 years of DMSP satellite observations during 2002 and 2003.

2. Data Set and Processing Approach

2.1. DMSP Ion Drift Meter and Special Sensor Precipitating Electron and Ion Spectrometer Data

[7] The DMSP satellites sample polar regions at ~835 km altitude along orbits at fixed local time planes. The orbital period is approximately 100 min. One of the satellites (F13) has a near dawn-dusk orbit and two (F14 and F15) have 0930–2130 MLT orbits. The events have been separated into four groups according to their flux tube–integrated ionospheric conductivity: (1) the footprint regions in both hemispheres are in sunlight (sunlit-sunlit); (2) the Northern Hemisphere is in sunlight while the Southern Hemisphere is in darkness (sunlit-dark); (3) the Northern Hemisphere is in darkness while the Southern Hemisphere is in sunlight (dark-sunlit); and (4) considered regions in both hemispheres are in darkness (dark-dark). We consider the observations to be in "darkness" when they are taken at solar zenith angles (SZA) $\geq 100^\circ$ and term them "sunlit" when the observations have SZA $< 100^\circ$ [*Schlegel*, 1988]. The SZA and MLT for each orbit segment in the Northern Hemisphere have been determined at the crossing point between the orbit and 65° MLAT, and the SZA in the Southern Hemisphere has been determined at the conjugate footprint (MLAT = −65°, and the MLT is the same as in the Northern Hemisphere). Group 1 can be classified as the cases with high conductance, groups 2 and 3 can be classified as cases with medium integrated conductance, and group 4 can be classified as those with low conductance. Figure 1 shows the duskside MLT distribution of the number of satellite passes in the Northern Hemisphere during 2002 and 2003 separately for these four conditions. The data have been further classified into "quiet" ($Kp < 3$) and "disturbed" ($Kp \geq 3$) geomagnetic conditions. The DMSP satellite tracks are confined to the MLT band of

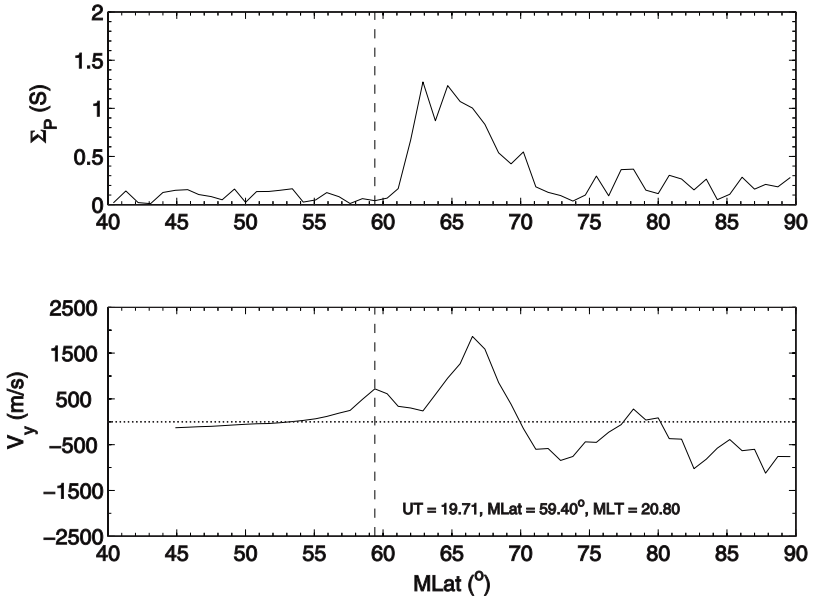

Figure 2. Examples of the latitude profile of the ionospheric convection velocity (V_y) and conductivity (Σ_P) obtained from DMSP F15 on 20 December 2003. The enhanced sunward (positive) plasma drift between 55° and 61° is the SAPS. The peak velocity is indicated by the dashed line. The UT, MLAT, and MLT where the SAPS velocity peak occurs are also given.

1500–2200 MLT, which covers the most probable location of SAPS except that part around the midnight MLT sector [e.g., *Karlsson et al.*, 1998; *Foster and Vo*, 2002]. As expected, the sunlit-sunlit and dark-dark orbits do not cover all the MLT sectors, with the former confined to the earlier MLT and the latter confined to the later MLT. Under both quiet and disturbed conditions the sunlit-dark satellite orbit sample numbers peak around 1800–1900 MLT, and the dark-sunlit samples peak around 1900–2000 MLT.

[8] Among various scientific instruments onboard, the instruments of primary interest in this study are the ion drift meter (IDM) and the electron spectrometers (Special Sensor Precipitating Electron and Ion Spectrometer (SSJ/4)). The ion drift velocities in the horizontal and vertical directions perpendicular to the satellite track are derived from the IDM data [*Rich and Hairston*, 1994]. The DMSP SSJ/4 instruments monitor the energy flux of electrons and ions in the range of 30 eV to 30 keV that precipitate from the Earth's magnetosphere [*Hardy et al.*, 1984]. *Robinson et al.* [1987] have described the relationship relating the energy flux and the average energy of the electrons with the height-integrated ionospheric conductivity.

[9] For this study, SAPS are defined as clearly identifiable sunward ion flows in the subauroral and premidnight region. A threshold of SAPS velocity greater than 100 m/s is used for selection. The subauroral region is found automatically by computing the auroral Pedersen conductance along the DMSP path and determining the peak conductance, then stepping equatorward until the conductance is reduced to 0.2 times the peak value or 1 S, whichever is smaller. The selected orbits are further visually inspected to fully satisfy the above criteria. As an example, Figure 2 shows the latitude profile of the ionospheric convection (bottom) and the Pedersen conductivity (top) due to particle precipitation. The large conductivity due to particle precipitation between 61° and 71° MLAT represents the auroral oval, and the large sunward ion flow in this region is the auroral plasma convection. The enhanced westward plasma drift equatorward of the auroral precipitation is the SAPS, whose peak velocity is indicated by the vertical dashed line. Only the SAPS observations in the Northern Hemisphere are considered in this study, and the interhemispheric comparison will be left for future studies.

[10] Two years of DMSP measurements during 2002–2003 have been processed, and 7760 SAPS events are picked out. An equal number of events exists for sunlit (3880 events) and dark conditions (3880 events). The time (universal time (UT)), position (MLT and MLAT), and magnitude of the peak velocities of SAPS are recorded for each event. If not stated differently, the MLAT, MLT, and velocity in the following sections are all described for those at the position where the SAPS velocity peaks. Figure 3 shows the MLT distribution of the number of the SAPS events under quiet and disturbed conditions separately for the four illumination conditions, as described earlier. The SZA are calculated at the conjugate positions in both hemispheres where the SAPS velocity peaks in magnitude. The SAPS events are observed generally during 1500–2200 MLT. For quiet and disturbed conditions both the sunlit-dark and dark-sunlit (i.e., medium-conductivity) SAPS event numbers peak around 1900–2000 MLT. The sunlit-sunlit (i.e., high-conductance) and dark-dark (i.e., low-conductance) SAPS events cover the earlier and later MLT hours.

2.2. AMIE-Derived CPCP Data

[11] The high-latitude ionospheric potential can be described by empirical relationships that relate geomagnetic conditions with solar wind drivers [e.g., *Weimer*, 1996; *Papitashvili and Rich*, 2002] and data assimilative models that ingest a large amount of observations into a background model [e.g., *Kamide et al.*, 1981; *Richmond*, 1992]. As

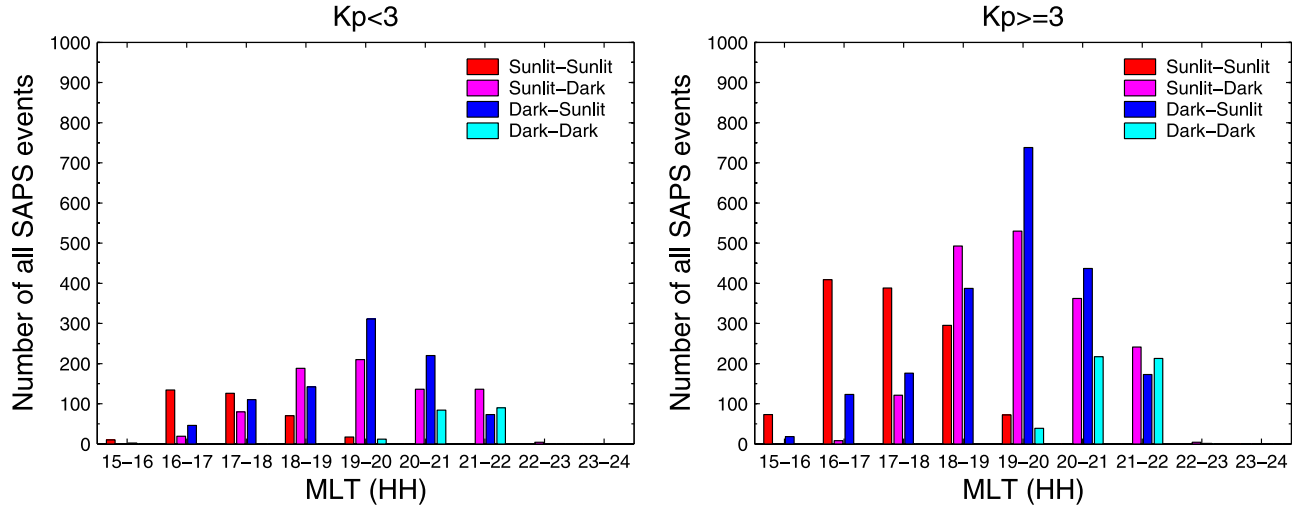

Figure 3. Distribution of the SAPS events as a function of MLT for two different geomagnetic activity levels, separately for four illumination cases (as in Figure 1).

compared to empirical models, the assimilative model can provide more realistic patterns [e.g., *Kihn et al.*, 2006]. Since the assimilative mapping of ionospheric electrodynamics (AMIE) technique is used extensively in the scientific community, we have employed AMIE to produce the high-latitude CPCP at 1 min resolution to study its relationship with the SAPS velocity. The global magnetometer data, the available interplanetary magnetic field, solar wind, hemispheric power index, $F_{10.7}$, and *Dst* data are used as inputs into the AMIE model [*Ridley and Kihn*, 2004]. A comparison of AMIE-produced CPCP to the other models has been performed by *Ridley* [2005], where the advantages of AMIE are stated.

3. Statistical Results

[12] The large number of SAPS events during the 2 years considered (7760 events) is a good basis for studying the statistical properties of SAPS in the Northern Hemisphere. The variations of SAPS with the solar illumination, geo-

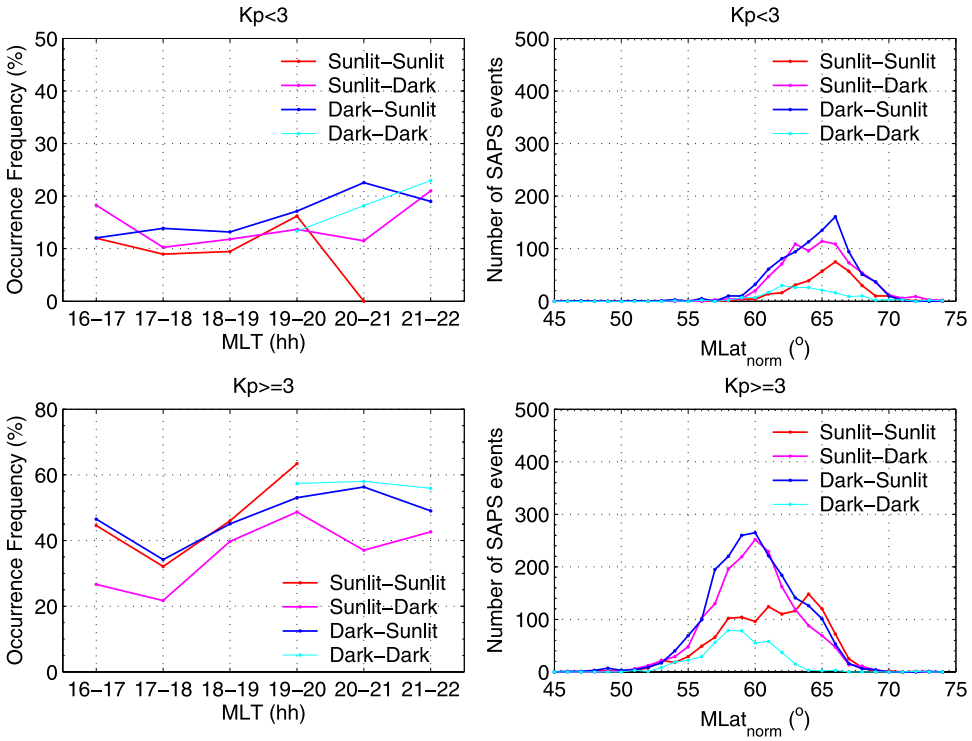

Figure 4. (left) The occurrence frequency of SAPS as a function of MLT, separately for four cases: (1) NH sunlit, SH sunlit; (2) NH sunlit, SH dark; (3) NH dark, SH sunlit; and (4) NH dark, SH dark. (right) The number of events as a function of MLAT. The top plots are for $Kp < 3$ and the bottom plots are for $Kp \geq 3$. The MLAT effect has been normalized to that at 2100 MLT (see text for the normalization).

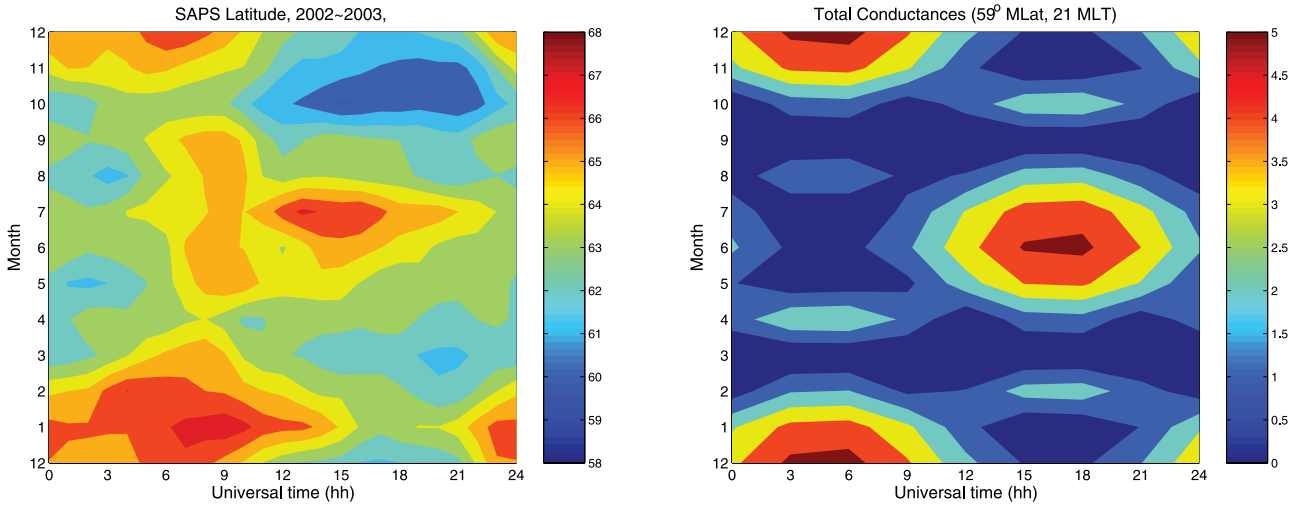

Figure 5. (left) The contour plot of the seasonal variation of the SAPS MLAT versus UT. (right) The contour plot of the seasonal UT variations of flux tube–integrated Pedersen conductances, in S, caused by solar irradiation at the conjugate footprints, ±59° MLAT and 2100 MLT.

magnetic activity, and CPCP have been studied in the following sections.

3.1. SAPS Location and Flux Tube–Integrated Conductivity

[13] For the purpose of this study the SAPS are binned by magnetic local time (1 h) and then separated into four groups according to the solar illumination conditions at the conjugate footprints in both hemispheres. The data are further classified into two groups corresponding to two different geomagnetic activity levels. The 1500–1600 MLT and 2200–2300 MLT sectors have been neglected because of the increasing uncertainty from the relatively limited number of data points. The number of events has been normalized to the number of DMSP orbits for each bin in local time. Figure 4 (left) shows the occurrence frequency of SAPS events as a function of MLT for sunlit and dark conditions under both quiet ($Kp < 3$, top) and disturbed ($Kp \geq 3$, bottom) conditions. The occurrence frequency has been derived by dividing the histogram in Figure 3 by the number of all passes shown in Figure 1. The curves reflect the percentage of DMSP passes that measure SAPS under different conditions. The occurrence frequency is much higher under disturbed conditions than during quiet times. For sunlit-sunlit (i.e., high-conductance) and dark-sunlit (i.e., medium-conductance) conditions, SAPS exhibit occurrence peaks around 1900–2000 MLT and 2000–2100 MLT irrespective of the geomagnetic activity levels. For both sunlit-dark (i.e., medium-conductance) and dark-dark (i.e., low-conductance) conditions SAPS occurrence rates peak around 2100–2200 MLT under quiet conditions, while both shift earlier to 1900–2000 MLT under disturbed conditions. From Figure 4 (left) the effect of the flux tube–integrated conductivity on the SAPS MLT distribution is not clear and seems inconclusive.

[14] Previous studies indicated that the SAPS' MLAT changes linearly with MLT [*Foster and Vo*, 2002]. We have adopted the relationship $\text{MLAT}_{\text{norm}} = \text{MLAT} + 0.8(\text{MLT} - 21)$ to normalize the SAPS MLAT in different MLT sectors to that at 2100 MLT, as proposed by *Huang and Foster* [2007]. The SAPS are binned in magnetic latitude (1°) and then classified into four groups according to the daylight and darkness in both hemispheres. The data are further separated into two groups for two different geomagnetic activity levels. Figure 4 (right) shows the resulting distributions of the number of the SAPS events as a function of MLAT, reflecting the most probable MLAT locations for sunlit and dark conditions under quiet and disturbed conditions. SAPS shift to lower latitudes when the magnetic activity increases. The solar illumination difference in the magnetic latitude of SAPS is also more prominent under disturbed conditions than during quiet times. Under quiet conditions the distribution peaks at 66° MLAT, which is the same for the high and medium flux tube–integrated conductivity conditions. For the low-conductance condition, the SAPS peak at a lower latitude, around 62° MLAT. Under disturbed conditions the most likely location tends to occur at ~64° MLAT for the high-conductance condition, ~60° MLAT for the medium-conductance condition, and ~58° MLAT for the low-conductance condition. A t-test has been performed to see whether these groups have the same mean latitude when the standard deviations are unknown but assumed to be equal. The results show that they have totally different mean MLATs, with the MLAT difference between high and the low conductance being 1.9° ~ 2.7° and the MLAT difference between the medium and the low conductance being 0.79° ~ 1.4°.

[15] To further visualize a direct relation of the MLAT distribution to the flux tube–integrated conductivity due to solar illumination, Figure 5 shows the distribution of magnetic latitudes of the SAPS (left) and the flux tube–integrated Pedersen conductance (right) at ±59° MLAT and 2100 MLT, in a month versus universal time coordinate frame. For the estimation of the Pedersen conductivity, we have made use of the approach by *Schlegel* [1988]. When comparing the MLAT and the integrated conductivity we find a clear correlation of poleward shift of SAPS location at times of higher conductance. In sections 3.2 and 3.3 we will combine conditions 2 and 3 into one group since both of them reflect the medium-conductance conditions.

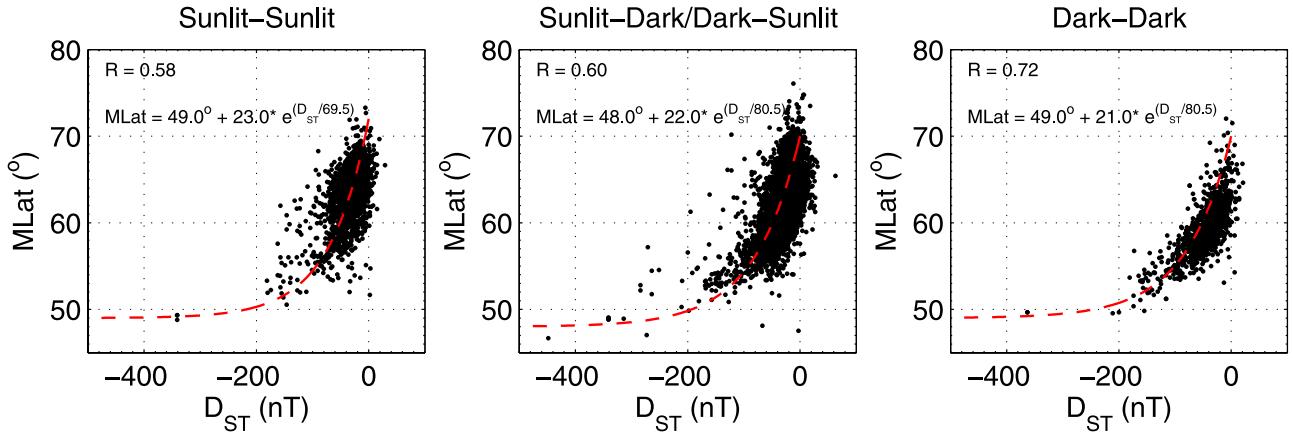

Figure 6. The normalized MLAT of the SAPS peak velocity as a function of *Dst* for three conditions: (left) both hemispheres are in sunlight, (middle) one is in sunlight while the other is in darkness, and (right) both are in darkness. The dashed red curve represents an exponential fit to the data. The correlation coefficient and the fit function are also given.

3.2. Correlation of SAPS' Latitude With *Dst*

[16] A relationship between the *Dst* value and latitudes where the SAPS velocity peaks in magnitude is sought. The *Dst* has been regarded as the suitable geomagnetic activity index for describing the location of SAPS [*Huang and Foster*, 2007]. To remove the MLAT variations due to MLT changes, the MLAT has been normalized to that in the 2100 MLT sector [*Huang and Foster*, 2007]. Figure 6 depicts the relationship between the *Dst* and the normalized magnetic latitude of the SAPS separately for sunlit and dark conditions in both hemispheres. A reasonable correlation can be obtained between the latitude of SAPS and the *Dst* value when using an exponential relation. The equatorward shift of the SAPS MLAT with the *Dst* tends to slow down at high activity, and the SAPS MLAT tends to occur around 48° – 49° MLAT at very high activity. We obtain the *Dst* versus MLAT relationship from the fitted function for the high-conductance condition, MLAT = 49° + $23e^{Dst/69.5}$; for the medium-conductivity condition, MLAT = 48° + $22e^{Dst/80.5}$; and for the low-conductivity condition, MLAT = 49° + $21e^{Dst/80.5}$.

3.3. Response of SAPS Velocity to the High-Latitude Electric Field

[17] The CPCP is a convenient quantity that characterizes the strength of the high-latitude electric field, which is obtained by subtracting the minimum potential from the maximum potential value. The correlation has been limited to $Kp \leq 6$ in our study in order to avoid increasing errors from relatively small numbers of samples at extreme activity. Figure 7 shows the relationship between the CPCP produced by AMIE and the observed SAPS peak velocities separately for three levels of conductivity conditions. The top plots show the relationship between the SAPS peak velocities and the CPCP without any time delay between the quantities. The plots below reflect the results when averaging CPCP over three different intervals of 15, 30, or 60 min preceding the time of the peak SAPS velocities, in order to see the integrated effects of the CPCP on the SAPS. The main features emerging from Figure 7 can be summarized as follows.

[18] 1. The best correlation can be found for the CPCP averaged over an interval of 15 min yielding a correlation coefficient R = 0.56, R = 0.43, and R = 0.41 for high, medium, and low integrated conductance conditions, respectively. There occurs some scattering of the SAPS velocity about the regression line, and the correlation is not as good for the latter two cases, which will be discussed in section 4.3.

[19] 2. It seems that a somewhat smaller slope is derived for high conductances as compared to medium and low conductances. This indicates that the magnitude of the SAPS in response to the solar wind input is stronger when the integrated conductivity is low than when the conductivity is high.

[20] The high integrated conductivity depresses the magnitude of SAPS. This is shown in more detail in Figure 8, where a contour plot of the peak SAPS velocities versus the 15-min-averaged CPCP and flux tube–integrated Pedersen conductivity due to solar illumination at conjugate footprints of the peak SAPS is shown. The increase of the SAPS peak velocity with the CPCP is stronger for smaller conductivity. The largest SAPS velocities can be found for the smallest conductance and the largest CPCPs. The maximum to minimum ratio of the SAPS velocity is found to be amounting to around 3.0.

3.4. SAPS Velocity and Flux Tube–Integrated Conductivity

[21] To further visualize a direct relation of the SAPS velocity to the solar illumination conditions, Figure 5 shows the distribution of the SAPS velocity (left) and the flux tube–integrated Pedersen conductance due to solar illumination (right) at ±59° MLAT and 2100 MLT, in a month versus universal time coordinate frame. When comparing the velocity and the integrated conductivity we find a clear correlation of larger SAPS velocity at times of smaller conductances. The SAPS velocities vary by a factor of ∼2.

4. Discussion

[22] In this study, we have investigated certain features of SAPS in the Northern Hemisphere. Some interesting results

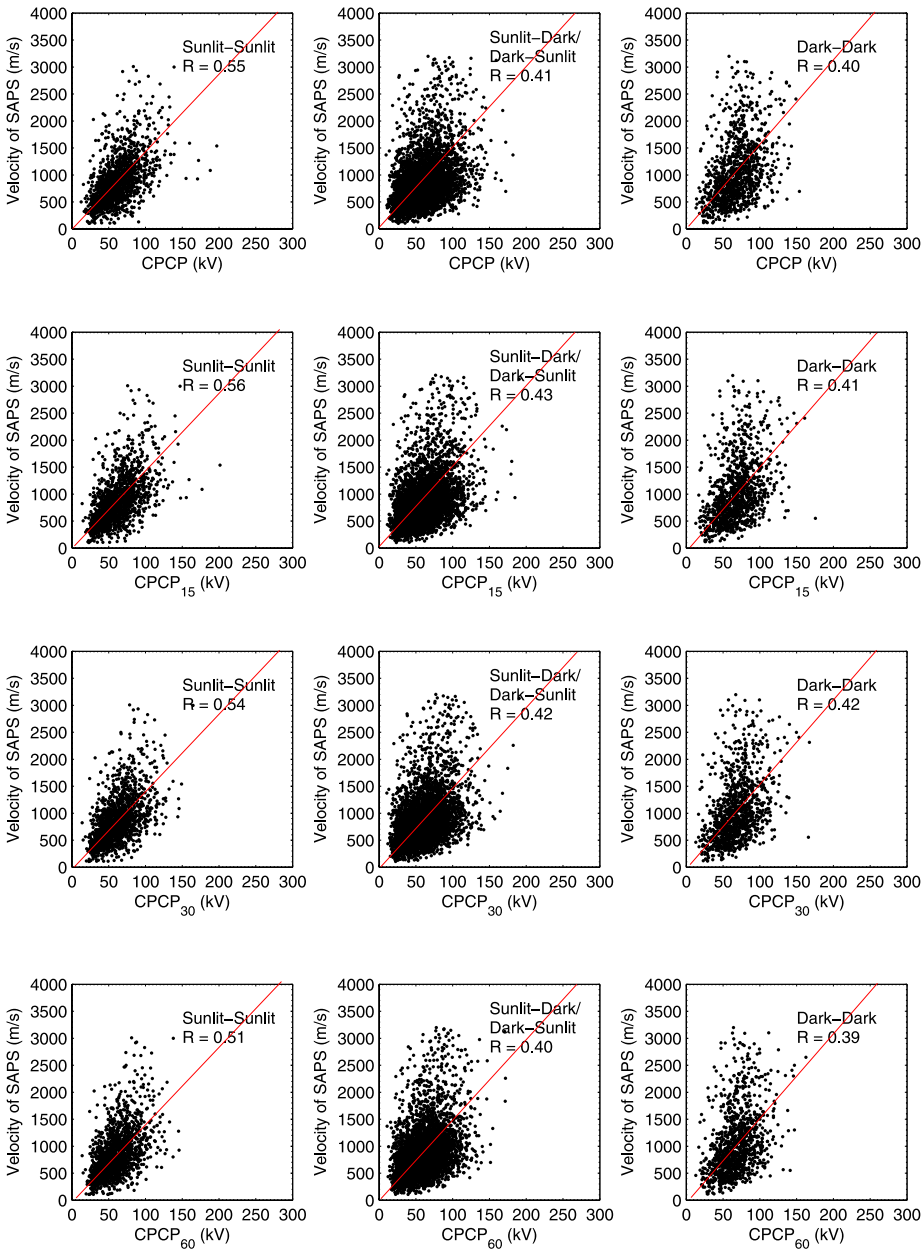

Figure 7. The SAPS peak velocity as a function of the cross–polar cap potential (CPCP) for three conditions: (left) both hemispheres are sunlit, (middle) one is sunlit while the other is dark, and (right) both are dark. From top to bottom the CPCP values are averaged over 0, 15, 30, and 60 min prior to the time of SAPS peak velocity observation. The red line represents the linear fit to the data. The correlation coefficients are given in the frames.

on the spatial distribution of the SAPS and their variations with the solar illumination, CPCP, and geomagnetic activity are obtained.

4.1. SAPS Location and Flux Tube–Integrated Conductivity

[23] Previous statistical studies have shown that the SAPS occur predominantly in the premidnight sector with the maximum probability locating during 2000–2300 MLT [e.g., *Karlsson et al.*, 1998; *Figueiredo et al.*, 2004]. This is because in the evening sector the ion precipitation boundary is located earthward (equatorward) of the electron precipitation, while in the morning sector the situation is reversed [*Anderson et al.*, 2001]. Precipitating electrons are known to be more efficient in enhancing the ionospheric conductivity than ions. The three DMSP satellite tracks are mainly confined to the 1600–2200 MLT sector (see Figure 1), which covers the most probable locations of SAPS, except for the 2200–2300 MLT sector [*Karlsson et al.*, 1998]. The present study cannot discriminate the effect of the flux tube–integrated conductivity on the SAPS MLT distribution. Although, previous model results showed by using a self-consistent simulation of the ring current protons that the locally reduced conductance in the dusk sector

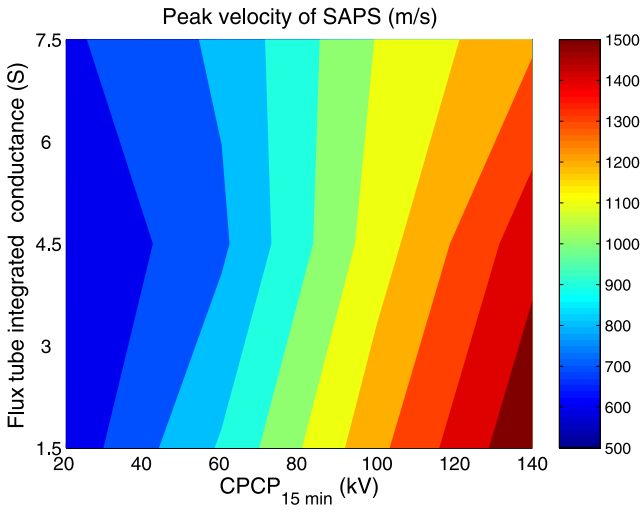

Figure 8. The variation of the SAPS peak velocity plotted versus the 15-min-averaged CPCP and the flux tube–integrated Pedersen conductance, in S, caused by solar irradiation at the conjugate footprints of the SAPS MLAT.

causes the peak R2 FACs to extend somewhat eastward [*Zheng et al.*, 2008] and the lower ionospheric conductance results in a proton emission peak located more eastward than for higher conductance [*Ebihara and Fok*, 2004].

[24] An important result of this study is that the SAPS latitude varies with the flux tube–integrated conductivity, and this variation becomes more prominent at higher magnetic activity. From Figure 4 (right) and Figure 5 one can also see that there is an equatorward shift of SAPS when the integrated conductivity is decreased. This matches the general findings of *Liemohn et al.* [2005], who showed that when the conductance is reduced, the electric field is increased and the ring current particles can be injected to lower L shells, or lower latitudes. Further, earlier findings showed that the solar illumination can influence the position of the auroral oval. In the premidnight sector, the auroral oval expands in case of darkness about 1.5° ∼ 2° equatorward [*Christiansen et al.*, 2002; *Wang et al.*, 2005a]. We can expect that the subauroral precipitation patterns show a similar expansion as the auroral oval.

4.2. SAPS Location and *Dst*

[25] There seems to be an exponential relationship between the SAPS MLAT and *Dst*, where the SAPS latitude tends to occur around ∼49° MLAT at high magnetic activity. Since the SAPS are almost collocated with the ionospheric horizontal currents, this result is consistent with our previous findings that the most equatorward location of the ionospheric horizontal currents tends to saturate for large *Dst* values [*Wang et al.*, 2008]. This exponential relationship differs from the analysis of *Huang and Foster* [2007], who found a linear relationship between the SAPS location and *Dst*. However, the *Huang and Foster* [2007] result is derived from four extreme magnetic storms, while our result is based on a larger set of SAPS events with *Kp* covering a much wider range.

[26] The SAPS MLAT-*Dst* relationship can also be regarded as a monitor for the location of the inner boundary of the ion plasma sheet and the location of the ring current peak since the SAPS are regarded to be collocated with them [*Anderson et al.*, 1993; *Goldstein et al.*, 2005; *Huang and Foster*, 2007]. The shift of SAPS location toward lower latitudes indicates that the ring current and plasma sheet ions move earthward. With increasing geomagnetic levels the magnetospheric convection electric field will get enhanced, which can drive the plasma sheet ions to move more deeply into the inner magnetosphere. However, when the magnetic activity increases above a certain value (*Dst* < −200 nT), the earthward movement of the ions tends to slow down and finally stops at about L = 2.2 R_E. This is most likely due to the increasing negative feedback between the ring current intensity and the loss processes, as the ring current moves closer to the Earth.

4.3. SAPS Velocity

[27] As explained in section 1 and in many previous studies [e.g., *Daglis and Kozyra*, 2002; *Kozyra and Liemohn*, 2003; *Liemohn and Kozyra*, 2003], the ring current is partially controlled by the high-latitude electric field. It is therefore expected that the velocity of the SAPS is also influenced by the polar cap potential difference. Several tests have been performed to examine the coupling between the SAPS and the high-latitude *E* field, as quantified by the CPCP. These include investigations on how the time history of the CPCP affects the SAPS velocity. Various delays of about 0, 10, 20, 30, and 60 min or averages over a time history of about 15, 30, and 60 min have been tested in our studies. The best correlation between the CPCP and SAPS velocity is obtained here when the CPCP is averaged over a time of 15 min prior to the SAPS measurement, representing the integrated effects of the CPCP on the plasma drifts over a time history of 15 min.

[28] Our results show the best correlation between SAPS velocity in daylight and the 15-min-averaged high-latitude CPCP (see Figure 7), indicating that the CPCP is one of the strong drivers of the SAPS. According to the generally accepted theory of the SAPS formation [e.g., *Anderson et al.*, 2001], the enhanced convection electric field can inject more ions into the ring current and inner magnetosphere, forming a larger azimuthal pressure gradient. The stronger R2 FACs will be generated by the enhanced misalignment between the large azimuthal pressure gradient and the orientation of the magnetic field flux tube. When the larger R2 FACs flow into the ionospheric region of low conductivity in the dusk sector, the electric field has to be increased to maintain the current continuity. Therefore, the enhanced poleward electric field causes the SAPS to be enhanced. When the conductivity is reduced, the electric field will be further enhanced, which in turn enhances the SAPS velocity. This explains our results that the CPCP causes stronger SAPS velocity at smaller conductance than at larger conductance (see Figures 7 and 8).

[29] The conductivity effect on the SAPS velocity is further validated in Figure 9, which shows the UT seasonal variations of SAPS velocity together with the estimated flux tube–integrated subauroral Pedersen conductivity due to solar illumination. The conductivity effect on the SAPS velocity has been discussed in previous modeling studies but has not been investigated utilizing observations. Our study indicates the coincidence of the smaller SAPS velocity with larger conductivity. This is consistent with the

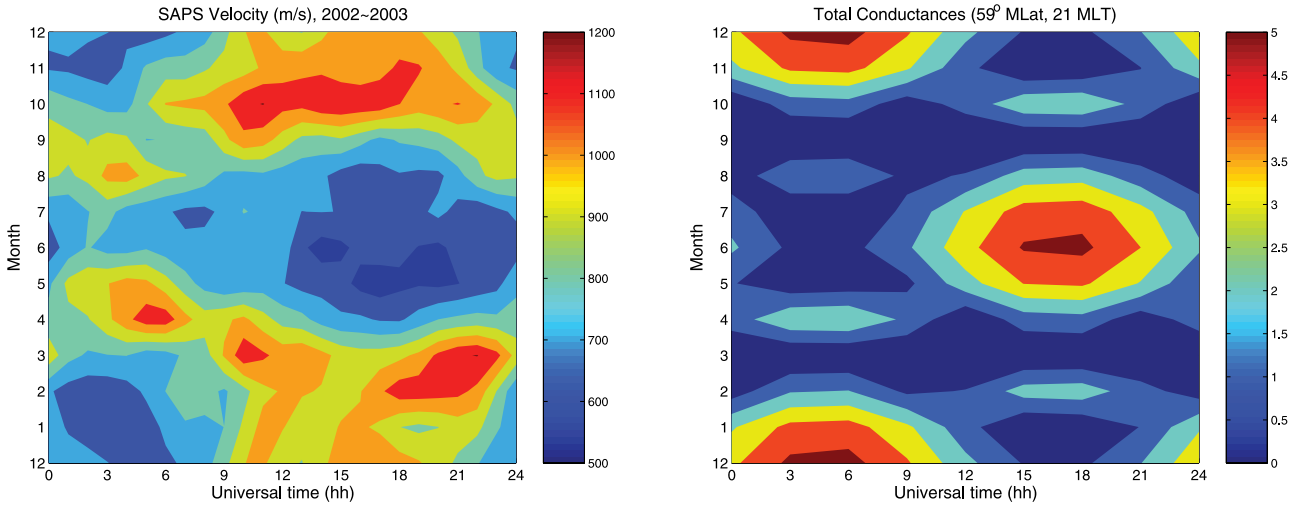

Figure 9. (left) The contour plot of the seasonal variation of the SAPS peak velocity versus UT. (right) The predicted seasonal UT variations of flux tube–integrated Pedersen conductance, in S, caused by solar irradiation at the conjugate footprints, ±59° MLAT and 2100 MLT.

previous results that the SAPS velocity is larger in winter as compared to summer [*Koustov et al.*, 2006] and also confirms the model result that the SAPS velocity decreases as the conductivity increases [*Zheng et al.*, 2008].

[30] In Figure 7, there is significant scattering of the SAPS velocity around and above the regression line when the conductivity is medium and low. Strong SAPS velocities (≥1500 m/s) can be found even when CPCP is less than 100 kV. *Karlsson et al.* [1998] also noticed that strong subauroral electric fields can be observed during relatively low magnetic activity in winter. A reason for these strong SAPS velocities might be substorm injections [e.g., *Ganushkina et al.*, 2001; *Carpenter and Smith*, 2001; *Goldstein et al.*, 2005]. To test this hypothesis, we have divided the data set of $Kp = 4$ and 60 kV ≤ CPCP ≤ 90 kV into two groups depending on the magnitude of the velocity (V). The events with $V \geq 1500$ m/s go into the group "larger velocity", and those with $V < 1500$ m/s go into the group "smaller velocity" (17 events in the larger velocity group and 112 events in the smaller velocity group). For each group the occurrence frequency has been determined for different ranges of the *AL* index produced by the AMIE technique,

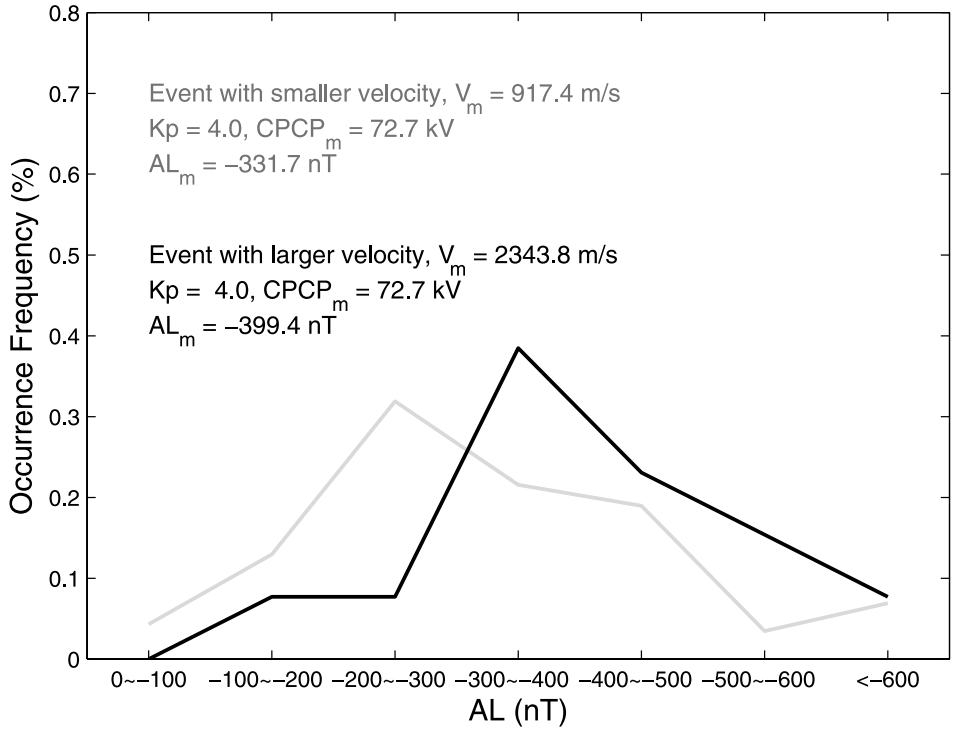

Figure 10. The occurrence frequency of the SAPS events versus the *AL* index for two groups of events both in darkness and at $Kp = 4$.

which are averages over 15 min. These are shown in Figure 10. The averaged CPCP for each group is approximately the same (~73 kV), but the average velocity varies by a factor of 2.6. In addition, the *AL* index is 1.3 times larger for the larger velocity group than for the smaller velocity group, thus providing support to the idea that the substorm particle injection may also play an important role in the enhancement of the SAPS velocity. Substorms tend to occur in darkness [e.g., *Lyons*, 1996; *Akasofu*, 2004; *Wang et al.*, 2005b]. The rapid sunward motion of geomagnetic field lines during the substorm dipolarization process can inject magnetotail plasma earthward and energize it. Injections will produce sharp increases in ring current particle fluxes; thus, the SAPS velocity will get increased [e.g., *Ganushkina et al.*, 2001; *Carpenter and Smith*, 2001; *Daglis and Kozyra*, 2002; *Goldstein et al.*, 2005]. We regard this as an important mechanism for producing high SAPS velocities for low CPCP values.

5. Summary

[31] The statistical analysis of a large number of SAPS events from DMSP observations has revealed several interesting features, which can be summarized as follows.

[32] 1. Solar illumination, and with it the subauroral ionospheric flux tube–integrated conductance, in both hemispheres has an effect on the most probable latitude of SAPS occurrence. SAPS tend to occur more equatorward for larger flux tube–integrated conductivity. This solar illumination effect on the SAPS location is more prominent under magnetically disturbed conditions.

[33] 2. The magnetic latitude of the SAPS peak velocity has a clear exponential relationship with the *Dst* value, such that the SAPS is never observed equatorward of about 47° MLAT or at an L value of <2.2 R_E. This is most likely due to the increasing negative feedback effect between the ring current strength and the loss processes, when the ring current region moves closer to the Earth.

[34] 3. The high-latitude electric field, represented by the cross–polar cap potential averaged over 15 min prior to the SAPS event, correlates well with the magnitude of the SAPS peak velocity. The proportionality factor between the CPCP and the SAPS velocity is larger when the integrated conductivity is smaller. This indicates that the integrated conductivity plays a strong role in the development of the SAPS.

[35] 4. The observations indicate that there is a good correlation between the flux tube–integrated Pedersen conductivity due to solar illumination and the magnitude of the SAPS velocity, thus offering support to previous model predictions.

[36] In our future work observations from radar will be included to fill the midnight gap in the MLT coverage, and a much larger number of data sets will be utilized to clarify the climatology and the interhemispheric comparison of the SAPS.

[37] **Acknowledgments.** We thank the Center for Space Sciences at the University of Texas at Dallas and the U.S. Air Force for providing the DMSP IDM plasma data and the Space Physics Interactive Data Resource (SPIDR) for providing the DMSP SSJ/4 data. The WDC C2 for Geomagnetism at Kyoto are greatly acknowledged for providing the geomagnetic indices data. This work is supported by the AFOSR grant FA 9550-07-1-0434, NSF grant ATM0639336, and National Nature Science Foundation of China (40604017).

[38] Amitava Bhattacharjee thanks Asgeir Brekke and another reviewer for their assistance in evaluating this paper.

References

Akasofu, S.-I. (2004), Several "controversial" issues on substorms, *Space Sci. Rev.*, *113*, 1–40.

Anderson, P. C., R. A. Heelis, and W. B. Hanson (1991), The ionospheric signatures of rapid subauroral ion drifts, *J. Geophys. Res.*, *96*(A4), 5785–5792.

Anderson, P. C., W. B. Hanson, R. A. Heelis, J. D. Craven, D. N. Baker, and L. A. Frank (1993), A proposed production model of rapid subauroral ion drifts and their relationship to substorm evolution, *J. Geophys. Res.*, *98*(A4), 6069–6078.

Anderson, P. C., D. L. Carpenter, K. Tsuruda, T. Mukai, and F. J. Rich (2001), Multisatellite observations of rapid subauroral ion drifts (SAID), *J. Geophys. Res.*, *106*(A12), 29,585–29,599, doi:10.1029/2001JA000128.

Burke, W. J., A. G. Rubin, N. C. Maynard, L. C. Gentile, P. J. Sultan, F. J. Rich, O. de La Beaujardière, C. Y. Huang, and G. R. Wilson (2000), Ionospheric disturbances observed by DMSP at middle to low latitudes during the magnetic storm of June 4–6, 1991, *J. Geophys. Res.*, *105*(A8), 18,391–18,405, doi:10.1029/1999JA000188.

Carpenter, D. L., and A. J. Smith (2001), The study of bulk plasma motions and associated electric fields in the plasmasphere by means of whistler-mode signals, *J. Atmos. Sol. Terr. Phys.*, *63*, 1117–1132.

Christiansen, F., V. O. Papitashvili, and T. Neubert (2002), Seasonal variations of high-latitude field-aligned currents inferred from Ørsted and Magsat observations, *J. Geophys. Res.*, *107*(A2), 1029, doi:10.1029/2001JA900104.

Daglis, I. A., and J. U. Kozyra (2002), Outstanding issues of ring current dynamics, *J. Atmos. Sol. Terr. Phys.*, *64*, 253–264.

Ebihara, Y., and M.-C. Fok (2004), Postmidnight storm-time enhancement of tens-of-keV proton flux, *J. Geophys. Res.*, *109*, A12209, doi:10.1029/2004JA010523.

Fejer, B. G., and L. Scherliess (1998), Mid- and low-latitude prompt-penetration ionospheric zonal plasma drifts, *Geophys. Res. Lett.*, *25*(16), 3071–3074, doi:10.1029/98GL02325.

Figueiredo, S., T. Karlsson, and G. T. Marklund (2004), Investigation of subauroral ion drifts and related field-aligned currents and ionospheric Pedersen conductivity distribution, *Ann. Geophys.*, *22*, 923–934.

Foster, J. C., and H. B. Vo (2002), Average characteristics and activity dependence of the subauroral polarization stream, *J. Geophys. Res.*, *107*(A12), 1475, doi:10.1029/2002JA009409.

Foster, J. C., P. J. Erickson, A. J. Coster, J. Goldstein, and F. J. Rich (2002), Ionospheric signatures of plasmaspheric tails, *Geophys. Res. Lett.*, *29*(13), 1623, doi:10.1029/2002GL015067.

Galperin, Y., V. N. Ponomarev, and A. G. Zosimova (1974), Plasma convection in the polar ionosphere, *Ann. Geophys.*, *30*, 1–7.

Ganushkina, N. Y., T. I. Pulkkinen, V. F. Bashkirov, D. N. Baker, and X. Li (2001), Formation of intense nose structures, *Geophys. Res. Lett.*, *28*(3), 491–494, doi:10.1029/2000GL011955.

Garner, T. W., R. A. Wolf, R. W. Spiro, W. J. Burke, B. G. Fejer, S. Sazykin, J. L. Roeder, and M. R. Hairston (2004), Magnetospheric electric fields and plasma sheet injection to low L-shells during the 4–5 June 1991 magnetic storm: Comparison between the Rice Convection Model and observations, *J. Geophys. Res.*, *109*, A02214, doi:10.1029/2003JA010208.

Goldstein, J., J. L. Burch, B. R. Sandel, S. B. Mende, P. C:son Brandt, and M. R. Hairston (2005), Coupled response of the inner magnetosphere and ionosphere on 17 April 2002, *J. Geophys. Res.*, *110*, A03205, doi:10.1029/2004JA010712.

Hardy, D. A., L. K. Schmitt, M. S. Gussenhoven, F. J. Marshall, and H. C. Yeh (1984), Precipitating electron and ion detectors (SSJ/4) for the block 5D/flights 6-10 DMSP (Defense Meteorological Satellite Program) satellites: Calibration and data presentation, *Rep. AFGL-TR-84-0314*, Air Force Geophys. Lab., Hanscom Air Force Base, Mass.

Huang, C.-S., and J. C. Foster (2007), Correlation of the subauroral polarization streams (SAPS) with the *Dst* index during severe magnetic storms, *J. Geophys. Res.*, *112*, A11302, doi:10.1029/2007JA012584.

Jensen, J. W., and B. G. Fejer (2007), Longitudinal dependence of middle and low latitude zonal plasma drifts measured by DE-2, *Ann. Geophys.*, *25*, 2551–2559.

Kamide, Y., A. D. Richmond, and S. Matsushita (1981), Estimation of ionospheric electric fields, ionospheric currents, and field-aligned currents from ground magnetic records, *J. Geophys. Res.*, *86*(A2), 801–813.

Karlsson, T., G. T. Marklund, and L. G. Blomberg (1998), Subauroral electric fields observed by the Freja satellite: A statistical study, *J. Geophys. Res.*, *103*(A3), 4327–4341.

Kihn, E. A., R. Redmon, A. J. Ridley, and M. R. Hairston (2006), A statistical comparison of the AMIE derived and DMSP-SSIES observed high-latitude ionospheric electric field, *J. Geophys. Res.*, *111*, A08303, doi:10.1029/2005JA011310.

Koustov, A. V., R. A. Drayton, R. A. Makarevich, K. A. McWilliams, J.-P. St-Maurice, T. Kikuchi, and H. U. Frey (2006), Observations of high-velocity SAPS-like flows with the King Salmon SuperDARN radar, *Ann. Geophys.*, *24*, 1591–1608.

Kozyra, J. U., and M. W. Liemohn (2003), Ring current energy input and decay, *Space Sci. Rev.*, *109*, 105–131, doi:10.1023/B:SPAC.0000007516.10433.ad.

Liemohn, M. W., and J. U. Kozyra (2003), Lognormal form of the ring current energy content, *J. Atmos. Sol. Terr. Phys.*, *65*, 871–886, doi:10.1016/S1364-6826(03)00088-9.

Liemohn, M. W., J. U. Kozyra, M. F. Thomsen, J. L. Roeder, G. Lu, J. E. Borovsky, and T. E. Cayton (2001), Dominant role of the asymmetric ring current in producing the stormtime Dst^*, *J. Geophys. Res.*, *106*(A6), 10,883–10,904, doi:10.1029/2000JA000326.

Liemohn, M. W., A. J. Ridley, P. C. Brandt, D. L. Gallagher, J. U. Kozyra, D. M. Ober, D. G. Mitchell, E. C. Roelof, and R. DeMajistre (2005), Parametric analysis of nightside conductance effects on inner magnetospheric dynamics for the 17 April 2002 storm, *J. Geophys. Res.*, *110*, A12S22, doi:10.1029/2005JA011109.

Liou, K., P. T. Newell, D. G. Sibeck, and C. I. Meng (2001), Observation of IMF and seasonal effects in the location of auroral substorm onset, *J. Geophys. Res.*, *106*(A4), 5799–5810.

Lyons, L. R. (1996), Substorms: Fundamental observational features, distinction from other disturbances, and external triggering, *J. Geophys. Res.*, *101*(A6), 13,011–13,025.

Papitashvili, V. O., and F. J. Rich (2002), High-latitude ionospheric convection models derived from Defense Meteorological Satellite Program ion drift observations and parameterized by the interplanetary magnetic field strength and direction, *J. Geophys. Res.*, *107*(A8), 1198, doi:10.1029/2001JA000264.

Rich, F. J., and M. Hairston (1994), Large-scale convection patterns observed by DMSP, *J. Geophys. Res.*, *99*(A3), 3827–3844.

Richmond, A. D. (1992), Assimilative mapping of ionospheric electrodynamics, *Adv. Space Res.*, *12*(6), 59–68, doi:10.1016/0273-1177(92)90040-5.

Ridley, A. J. (2005), A new formulation for the ionospheric cross polar cap potential including saturation effects, *Ann. Geophys.*, *23*, 3533–3547.

Ridley, A. J., and E. A. Kihn (2004), Polar cap index comparisons with AMIE cross polar cap potential, electric field, and polar cap area, *Geophys. Res. Lett.*, *31*, L07801, doi:10.1029/2003GL019113.

Ridley, A. J., and M. W. Liemohn (2002), A model-derived storm time asymmetric ring current driven electric field description, *J. Geophys. Res.*, *107*(A8), 1151, doi:10.1029/2001JA000051.

Robinson, R. M., R. R. Vondrak, K. Miller, T. Dabbs, and D. A. Hardy (1987), On calculating ionospheric conductances from the flux and energy of precipitating electrons, *J. Geophys. Res.*, *92*(A3), 2565–2569.

Scherliess, L., and B. G. Fejer (1998), Satellite studies of mid- and low-latitude ionospheric disturbance zonal plasma drifts, *Geophys. Res. Lett.*, *25*(9), 1503–1506, doi:10.1029/98GL01032.

Schlegel, K. (1988), Auroral zone E-region conductivities during solar minimum derived from EISCAT data, *Ann. Geophys*, *6*, 129–138.

Southwood, D. J., and R. A. Wolf (1978), An assessment of the role of precipitation in magnetospheric convection, *J. Geophys. Res.*, *83*(A11), 5227–5232.

Spiro, R. W., R. A. Heelis, and W. B. Hanson (1978), Ion convection and the formation of the mid-latitude F region ionization trough, *J. Geophys. Res.*, *83*(A9), 4255–4264.

Spiro, R. W., R. H. Heelis, and W. B. Hanson (1979), Rapid sub-auroral ion drifts observed by Atmospheric Explorer C, *Geophys. Res. Lett.*, *6*(8), 657–660.

Wang, H., H. Lühr, and S. Y. Ma (2005a), Solar zenith angle and merging electric field control of field-aligned currents: A statistical study of the Southern Hemisphere, *J. Geophys. Res.*, *110*, A03306, doi:10.1029/2004JA010530.

Wang, H., H. Lühr, S. Y. Ma, and P. Ritter (2005b), Statistical study of the substorm onset: Its dependence on solar wind parameters and solar illumination, *Ann. Geophys.*, *23*, 2069–2079.

Wang, H., H. Lühr, A. J. Ridley, P. Ritter, and Y. Yu (2008), Storm time dynamics of auroral electrojets: CHAMP observation and the Space Weather Modeling Framework comparison, *Ann. Geophys.*, *26*, 555–570.

Weimer, D. R. (1996), A flexible, IMF dependent model of high-latitude electric potentials having "space weather" applications, *Geophys. Res. Lett.*, *23*(18), 2549–2552, doi:10.1029/96GL02255.

Yeh, H.-C., J. C. Foster, F. J. Rich, and W. Swider (1991), Storm time electric field penetration observed at mid-latitude, *J. Geophys. Res.*, *96*(A4), 5707–5721.

Zheng, Y., P. C. Brandt, A. T. Y. Lui, and M.-C. Fok (2008), On ionospheric trough conductance and subauroral polarization streams: Simulation results, *J. Geophys. Res.*, *113*, A04209, doi:10.1029/2007JA012532.

M. W. Liemohn and A. J. Ridley, Department of Atmospheric, Oceanic and Space Sciences, University of Michigan, Ann Arbor, MI 48109, USA.
H. Lühr, GeoForschungsZentrum, Potsdam, D-14473, Germany.
S. Y. Ma and H. Wang, School of Electronic Information, Wuhan University, Wuhan, 430079, China. (h.wang@whu.edu.cn)